ISSN 0020-1685, Inorganic Materials, 2021, Vol. 57, No. 11, pp. 1158–1166. © Pleiades Publishing, Ltd., 2021.
Russian Text © The Author(s), 2021, published in Neorganicheskie Materialy, 2021, Vol. 57, No. 11, pp. 1226–1234.

Crystal Structure, Luminescence, and Thermodynamic Properties of $Pb_{10-x}Eu_x(GeO_4)_{2+x}(VO_4)_{4-x}$ ($x = 0.1, 0.2, 0.3$) Substituted Apatites

L. T. Denisova[a, *], M. S. Molokeev[a, b], A. S. Aleksandrovskii[a, b], Yu. F. Kargin[c], E. O. Golubeva[a], and V. M. Denisov[a]

[a] *Siberian Federal University, Krasnoyarsk, 660041 Russia*
[b] *Kirensky Institute of Physics, Krasnoyarsk Scientific Center (Federal Research Center), Siberian Branch, Russian Academy of Sciences, Krasnoyarsk, 660036 Russia*
[c] *Baikov Institute of Metallurgy and Materials Science, Russian Academy of Sciences, Moscow, 119334 Russia*
**e-mail: ldenisova@sfu-kras.ru*

Received June 10, 2021; revised July 17, 2021; accepted July 19, 2021

Abstract—$Pb_{10-x}Eu_x(GeO_4)_{2+x}(VO_4)_{4-x}$ ($x = 0.1, 0.2, 0.3$) Eu-substituted lead germanatovanadates with the apatite structure have been prepared by solid-state reactions, via firing in air in the temperature range 773–1073 K, using oxides (PbO, Eu_2O_3, GeO_2, and V_2O_5) as starting materials. Using X-ray diffraction, we have determined the hexagonal cell parameters (sp. gr. $P6_3/m$) of the synthesized phases and refined their crystal structure (the atomic position coordinates, isotropic thermal parameters, and principal bond lengths in their structure are presented). We have measured the luminescence spectra of the $Pb_{10-x}Eu_x(GeO_4)_{2+x}(VO_4)_{4-x}$ ($x = 0.1, 0.2, 0.3$) apatites and shown that europium concentration has little effect on the shape of the luminescence spectra. Using experimental heat capacity data obtained for polycrystalline samples by differential scanning calorimetry in the temperature range 350–1050 K, we calculated the main thermodynamic functions of the Eu-substituted lead germanatovanadates.

Keywords: apatites, lead europium germanatovanadates, X-ray diffraction, structure, luminescence, high-temperature heat capacity

DOI: 10.1134/S0020168521110030

INTRODUCTION

Mixed oxide compounds with the apatite structure (sp. gr. $P6_3/m$) have long been attracting researchers and practitioners' attention [1–7] owing to their diverse physicochemical properties, which determine their potential practical applications [1, 8–11]. A characteristic feature of the apatites (having the general formula $[A(1)]_4[A(2)]_6(RO_4)_6X_2$) is the possibility of ion substitutions without substantial changes their structure. Substitutions make it possible to tailor the properties of known compounds with the apatite structure and obtain new materials [12, 13]. For example, partial substitution of rare-earth ions for Pb in $Pb_5(GeO_4)(VO_4)_2$ made it possible to obtain $Pb_{10-x}R_x(GeO_4)_{2+x}(VO_4)_{4-x}$ (R = rare earth, $x = 0–3$) apatites [5, 10, 14, 15]. According to studies of Pb-containing apatites, their structure has two structurally inequivalent positions: Pb1 (4*f*) and Pb2 (6*h*) [2, 11, 16, 17]. It is worth noting that the $Pb_{10-x}R_x(GeO_4)_{2+x}(VO_4)_{4-x}$ materials are the least studied among the substituted lead germanatovanadates with the apatite structure.

The objectives of this work were to synthesize $Pb_{10-x}Eu_x(GeO_4)_{2+x}(VO_4)_{4-x}$ ($x = 0.1, 0.2, 0.3$) Eu-substituted apatites and study their crystal structure and optical and thermodynamic properties.

EXPERIMENTAL

The $Pb_{10-x}Eu_x(GeO_4)_{2+x}(VO_4)_{4-x}$ apatites were prepared by solid-state reactions using oxides as starting materials (extrapure-grade PbO and V_2O_5, reagent-grade Eu_2O_3, and 99.999%-pure GeO_2). After calcination, appropriate amounts of the oxides were mixed by grinding in an agate mortar and pressed with no binder into pellets, which were then sequentially fired in air at 773, 873, 973 (10 h of holding at each temperature), and 1073 K (holding for 100 h). To drive the solid-state reactions to completion, the samples were reground every 10 h of firing and the resultant powders were pressed, as in a previous study [14]. The

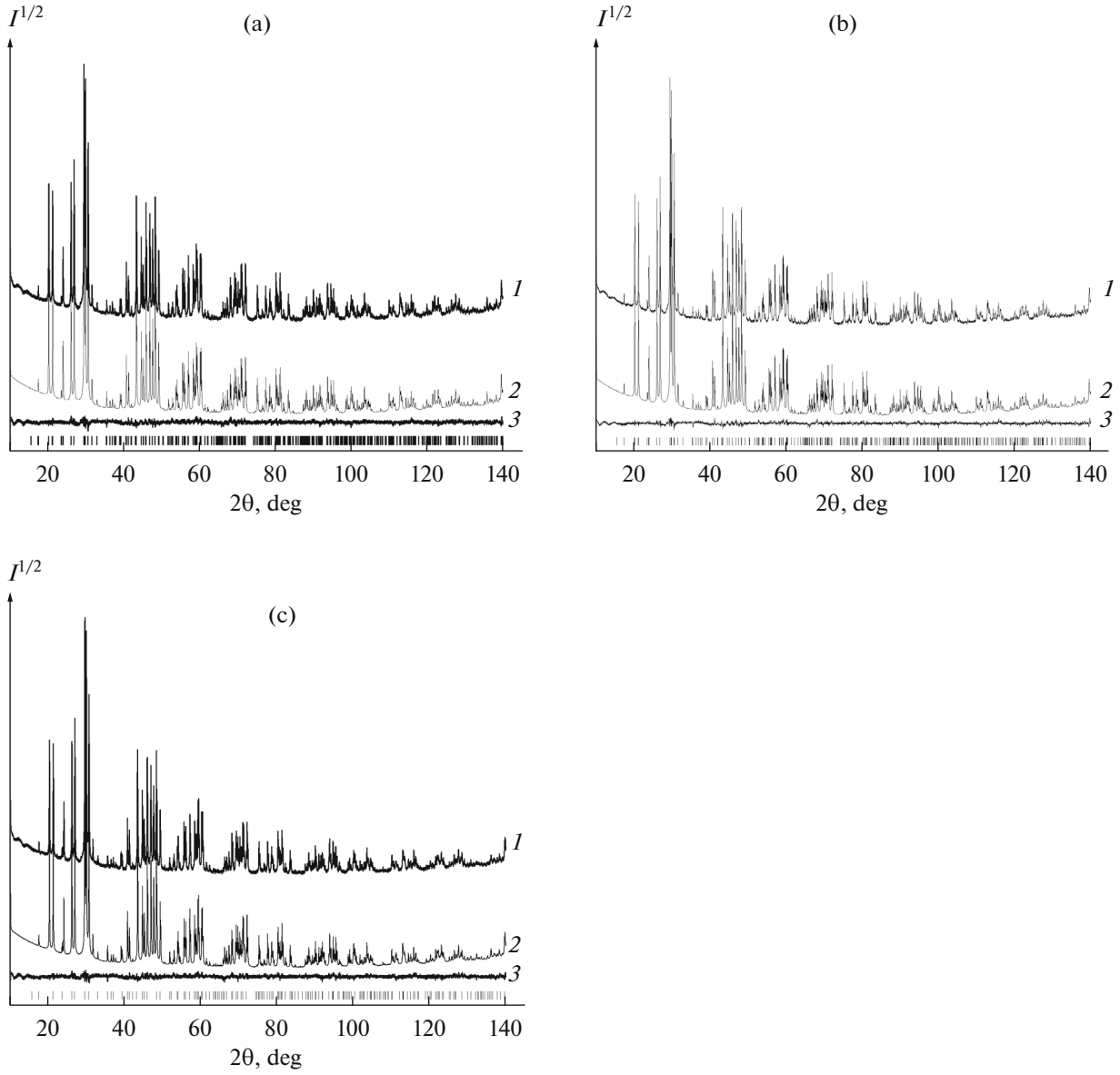

Fig. 1. (*1*) Raw X-ray diffraction data, (*2*) calculated profile, and (*3*) difference plot after refinement by the Rietveld method for $Pb_{10-x}Eu_x(GeO_4)_{2+x}(VO_4)_{4-x}$ with x = (a) 0.1, (b) 0.2, and (c) 0.3. The vertical tick marks show the calculated positions of allowed reflections.

phase composition of the samples thus prepared was determined by X-ray diffraction on a Bruker D8 Advance diffractometer (CuK_α radiation, scan step of 0.016°, counting time per data point of 2 s). The crystal structure of the samples was refined by the Rietveld method with TOPAS 4.2 software [18].

Luminescence spectra were measured at room temperature on a Horiba Jobin-Yvon T6400 spectrometer. Absorption spectra were obtained on a Shimadzu UV-3600 spectrophotometer.

The heat capacity of the synthesized polycrystalline apatite samples was determined by differential scanning calorimetry (DSC) (STA 449 C Jupiter thermoanalytical system, Netzsch, Germany). The experimental procedure was described in detail elsewhere [19]. The uncertainty in our measurements was within 2%.

RESULTS AND DISCUSSION

Figure 1 presents X-ray diffraction data for the synthesized apatites. It is seen that all of the samples are single-phase (there are no deviations in the difference plots).

All of the reflections in the X-ray diffraction patterns of the synthesized samples could be indexed in a

hexagonal structure (sp. gr. $P6_3/m$) with unit-cell parameters similar to those of $Pb_5(GeO_4)(VO_4)_2$ [2]. Because of this, the structure of this compound was used as an input model for Rietveld refinement. In accordance with the assumed chemical formula, the Pb/Eu ions were placed in the two inequivalent sites Pb1 and Pb2 with fixed site occupancies (Fig. 2).

For the only Ge/V site, we calculated the Ge : V ratio (also with allowance for the chemical formula), and the occupancies of these atoms were fixed during the refinement. The thermal parameters of all the atoms were taken to be isotropic. The refinement proceeded smoothly and yielded small agreement factors (Table 1, Fig. 1). The atomic position coordinates and principal bond lengths in the structure of the $Pb_{10-x}Eu_x(GeO_4)_{2+x}(VO_4)_{4-x}$ ($x = 0.1, 0.2, 0.3$) samples are listed in Tables 2 and 3, respectively.

Figure 3 illustrates the effect of europium content on the unit-cell parameters a and c, unit-cell volume V, and density of the $Pb_{10-x}Eu_x(GeO_4)_{2+x}(VO_4)_{4-x}$ apatites. It is seen that, as the degree of europium substitution for lead increases, a increases slightly, whereas c, d, and V decrease.

Rare-earth element substitution for Pb atoms is possible on both inequivalent Pb sites (Pb1 and Pb2). According to Yablochkova [5], praseodymium atoms substituting for Pb reside mainly on the Pb1 site, even though the effective charge on Pr^{3+} exceeds that on Pb^{2+}. Note that, if a substituent ion in the structure of hydroxyapatite has a larger charge, it occupies predominantly the Ca2 site, which is smaller in size [20].

Clearly, the observed decrease in the unit-cell volume and density of the $Pb_{10-x}Eu_x(GeO_4)_{2+x}(VO_4)_{4-x}$ apatites with increasing europium concentration can be accounted for by the difference in ionic radius between Pb^{2+} (1.35 Å) and Eu^{3+} (1.09 Å) and the difference in atomic mass (207.2 and 151.964 a. u. m., respectively).

Note that, because of the low Eu content ($x = 0.1$–0.3), we failed to determine the degree of Eu substitution for Pb on the Pb1 and Pb2 sites from X-ray diffraction data, so we measured luminescence spectra of the apatites under investigation.

Figure 4 shows luminescence spectra of the $Pb_{10-x}Eu_x(GeO_4)_{2+x}(VO_4)_{4-x}$ ($x = 0.1, 0.2, 0.3$) samples at an excitation wavelength of 464 nm, corresponding to the Eu^{3+} $^7F_0$–$^5D_2$ transition.

The spectra contain contributions from different Eu^{3+} luminescence bands and are dominated by the band corresponding to the crystal field-induced $^5D_0$–$^7F_2$ electric dipole transition and peaking at 612 nm, which points to distortion of inversion symmetry on the site occupied by the Eu^{3+} ions. However, the distortion is rather weak: the ratio of the peak intensities of the bands arising from the electric dipole and magnetic dipole transitions is about 3.4.

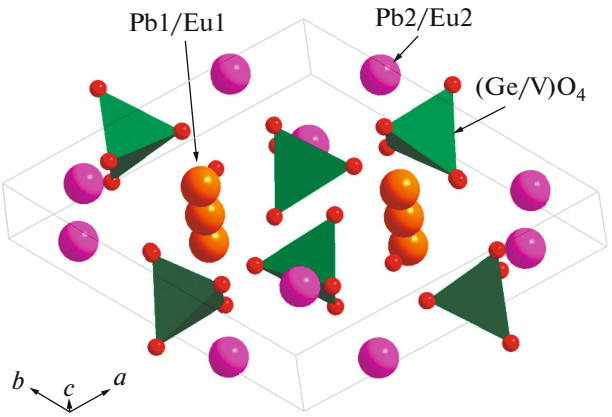

Fig. 2. Crystal structure of $Pb_{10-x}Eu_x(GeO_4)_{2+x}(VO_4)_{4-x}$.

A comparative analysis of the luminescence spectra of the three samples differing in Eu content demonstrates that the intensity distribution of individual bands and their shape change only slightly with increasing europium content. In particular, the intensity of the $^5D_0$–$^7F_1$ and $^5D_0$–$^7F_4$ bands rises in comparison with the $^5D_0$–$^7F_2$ band, whereas the intensity of the $^5D_0$–$^7F_0$ and $^5D_0$–$^7F_3$ bands remains unchanged. This suggests that the luminescence reabsorption effect has no influence on the spectra. Therefore, the observed slight changes in the shape of the lumines-

Table 1. Intensity data collection range, principal X-ray diffraction parameters, and structure refinement results for the $Pb_{10-x}Eu_x(GeO_4)_{2+x}(VO_4)_{4-x}$ ($x = 0.1, 0.2, 0.3$) samples

x	0.1	0.2	0.3
Sp. gr.	$P6_3/m$	$P6_3/m$	$P6_3/m$
a, Å	10.09108(4)	10.09120(4)	10.09127(4)
c, Å	7.39024(3)	7.38495(4)	7.38038(4)
V, Å^3	651.726(6)	651.274(6)	650.880(6)
Z	1	1	1
2θ, deg	5–140	5–140	5–140
R_{wp}, %	5.24	4.91	4.82
R_p, %	4.15	3.87	3.80
R_B, %	2.15	2.04	1.96
R_{exp}, %	2.70	2.73	2.73
χ^2	1.94	1.80	1.77

R_{wp}, R_p, R_B, and R_{exp} are the weighted profile, profile, Bragg, and experimental agreement factors, respectively; and χ^2 is the goodness-of-fit index.

Table 2. Atomic position coordinates and isotropic thermal parameters (Å^2) in the structure of the $Pb_{10-x}Eu_x(GeO_4)_{2+x}(VO_4)_{4-x}$ ($x = 0.1, 0.2, 0.3$) apatites

Atom	x	y	z	B_{iso}	Occupancy
			$x = 0.1$		
Pb1	1/3	2/3	0.0049(4)	1.00(4)	0.99
Eu1	1/3	2/3	0.0049(4)	1.00(4)	0.01
Pb2	0.25243(13)	0.0022(2)	1/4	1.03(4)	0.99
Eu2	0.25243(13)	0.0022(2)	1/4	1.03(4)	0.01
Ge	0.3987(4)	0.3846(4)	1/4	0.30(7)	0.35
V	0.3987(4)	0.3846(4)	1/4	0.30(7)	0.65
O1	0.3080(14)	0.4786(15)	1/4	2.2(2)	1
O2	0.5912(13)	0.4987(13)	1/4	2.2(2)	1
O3	0.3538(9)	0.2583(9)	0.0668(11)	2.2(2)	1
			$x = 0.2$		
Pb1	1/3	2/3	0.0053(4)	1.14(4)	0.98
Eu1	1/3	2/3	0.0053(4)	1.14(4)	0.02
Pb2	0.25328(12)	0.0030(2)	1/4	1.14(4)	0.98
Eu2	0.25338(12)	0.0030(2)	1/4	1.14(4)	0.02
Ge	0.3994(3)	0.3838(4)	1/4	0.30(7)	11/30
V	0.3994(3)	0.3838(4)	1/4	0.30(7)	19/30
O1	0.2993(13)	0.4707(14)	1/4	2.22(19)	1
O2	0.5903(13)	0.4971(13)	1/4	2.22(19)	1
O3	0.3533(9)	0.2599(9)	0.0711(10)	2.22(19)	1
			$x = 0.3$		
Pb1	1/3	2/3	0.0051(4)	1.17(4)	0.97
Eu1	1/3	2/3	0.0051(4)	1.17(4)	0.03
Pb2	0.25377(12)	0.0036(2)	1/4	1.12(4)	0.97
Eu2	0.25377(12)	0.0036(2)	1/4	1.12(4)	0.03
Ge	0.3999(3)	0.3844(4)	1/4	0.30(7)	23/60
V	0.3999(3)	0.3844(4)	1/4	0.30(7)	37/60
O1	0.3019(13)	0.4753(14)	1/4	2.25(19)	1
O2	0.5898(12)	0.5001(12)	1/4	2.25(19)	1
O3	0.3564(9)	0.2610(9)	0.0697(10)	2.25(19)	1

Table 3. Principal bond lengths (Å) in the structure of the $Pb_{10-x}Eu_x(GeO_4)_{2+x}(VO_4)_{4-x}$ ($x = 0.1$, 0.2, 0.3) apatites

		$x = 0.1$	
(Pb1/Eu1)–O1	2.542(9)	(Ge/V)–O1	1.615(9)
(Pb1/Eu1)–O2^{I}	2.861(9)	(Ge/V)–O2	1.692(9)
(Pb1/Eu1)–O3^{I}	2.904(8)	(Ge/V)–O3	1.756(8)
(Pb2/Eu2)–O1^{II}	2.810(13)		
(Pb2/Eu2)–O2^{III}	2.202(11)		
(Pb2/Eu2)–O3	2.630(8)		
(Pb2/Eu2)–O3^{IV}	2.553(8)		
		$x = 0.2$	
(Pb1/Eu1)–O1	2.572(9)	(Ge/V)–O1	1.635(8)
(Pb1/Eu1)–O2^{I}	2.855(9)	(Ge/V)–O2	1.678(9)
(Pb1/Eu1)–O3^{I}	2.919(8)	(Ge/V)–O3	1.716(8)
(Pb2/Eu2)–O1^{II}	2.733(12)		
(Pb2/Eu2)–O2^{III}	2.209(11)		
(Pb2/Eu2)–O3	2.621(8)		
(Pb2/Eu2)–O3^{IV}	2.577(7)		
		$x = 0.3$	
(Pb1/Eu1)–O1	2.546(8)	(Ge/V)–O1	1.652(8)
(Pb1/Eu1)–O2^{I}	2.878(8)	(Ge/V)–O2	1.673(8)
(Pb1/Eu1)–O3^{I}	2.890(8)	(Ge/V)–O3	1.723(8)
(Pb2/Eu2)–O1^{II}	2.768(12)		
(Pb2/Eu2)–O2^{III}	2.183(11)		
(Pb2/Eu2)–O3	2.627(8)		
(Pb2/Eu2)–O3^{IV}	2.578(7)		

Symmetry code: (i) $-x+1, -y+1, -z$; (ii) $-x+y, -x, -z+1/2$; (iii) $-y+1, x-y, -z+1/2$; (iv) $-y, -x+y, -z$.

cence spectra are attributable to the local changes induced in the crystal structure of the phases by the incorporation of europium ions. Analysis of the shape of the $^5D_0$–$^7F_0$ band, peaking at 578 nm, failed to provide any conclusive evidence for the presence of Eu^{3+} europium ions on two inequivalent sites. Comparison of the expected local environments of Eu^{3+} ions on these sites shows that the position corresponding to Pb2 ions, with Wyckoff notation 6*h* and local symmetry C_s, is highly asymmetric, whereas position Pb1, with Wyckoff notation 4*f* and local symmetry C_3, has moderate asymmetry. Thus, the luminescence spectra suggest that the Eu^{3+} ions reside predominantly in position Pb1.

Figure 5 shows excitation spectra of the Eu^{3+} ions in our samples at a luminescence wavelength of 612 nm (note that all of the spectra are identical).

$^5D_0$ excitation is most efficient on the $^7F_0$–$^5D_1$ transition, but excitation in the blue part of the emission range of GaN light-emitting diodes (on the $^7D_0$–$^5D_2$

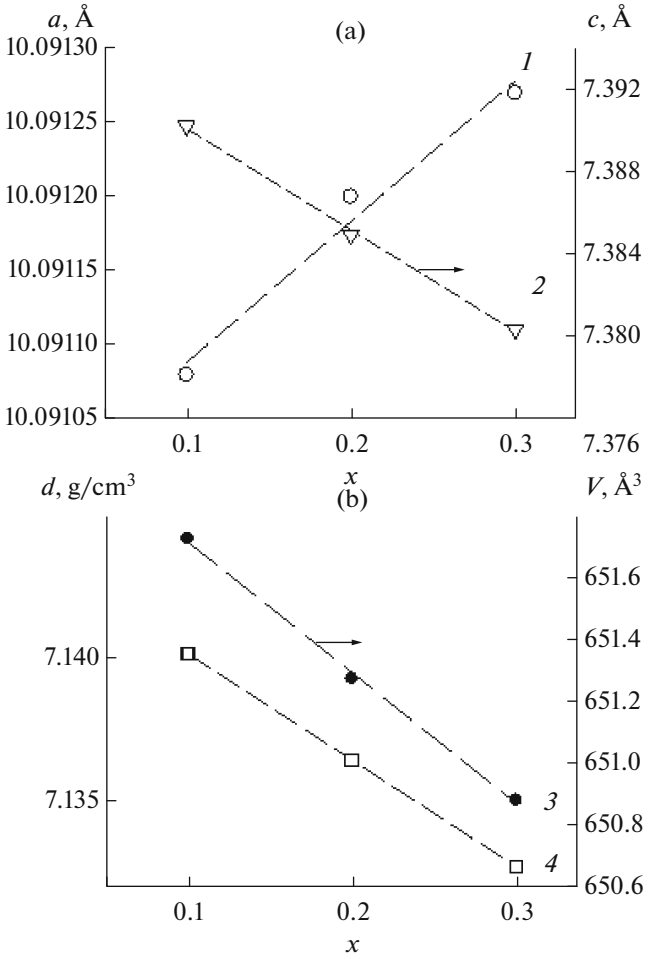

Fig. 3. Effect of composition on the unit-cell parameters a (*1*) and c (*2*), unit-cell volume V (*3*), and density d (*4*) of the $Pb_{10-x}Eu_x(GeO_4)_{2+x}(VO_4)_{4-x}$ apatites.

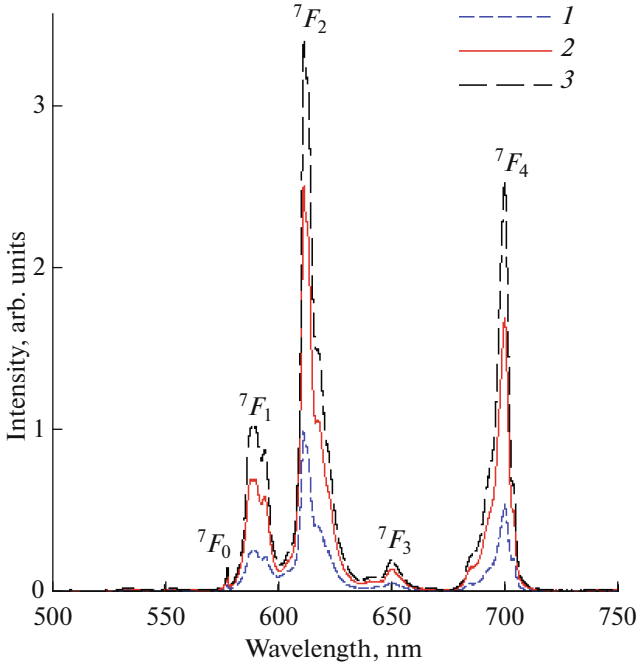

Fig. 4. Luminescence spectra of the $Pb_{10-x}Eu_x(GeO_4)_{2+x}(VO_4)_{4-x}$ apatites with x = (*1*) 0.1, (*2*) 0.2, and (*3*) 0.3.

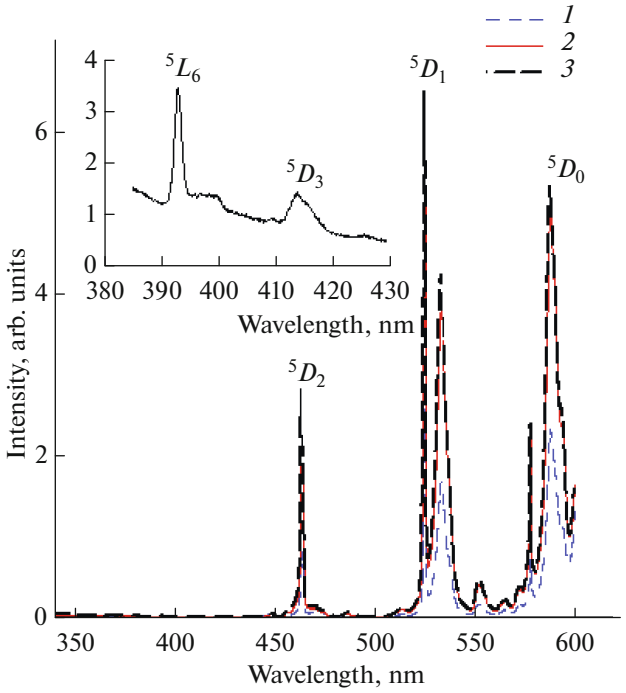

Fig. 5. Excitation spectra of the Eu^{3+} ions in $Pb_{10-x}Eu_x(GeO_4)_{2+x}(VO_4)_{4-x}$ with x = (*1*) 0.1, (*2*) 0.2, and (*3*) 0.3.

transition) is also rather efficient. In contrast, excitation in the violet and near-UV spectral regions has low efficiency. The increase in excitation efficiency around 300 nm, typically observed for europium ions in a number of hosts and related to excitation of a charge transfer band, is very small in the apatites studied here. As seen in the inset in Fig. 5, excitation through the $^5L_6$ level, which is also efficient in a number of hosts, occurs in our samples, but is far weaker than excitation through D states. One possible cause of this is nonradiative losses in relaxation processes from high-energy states to the $^5D_0$ state. The full width at half maximum (FWHM) of the spectral line corresponding to the $^7F_0$–$^5D_2$ transition in the photoluminescence excitation (PLE) spectrum is on the order of 2 nm, without any signs of broadening that might be expected for a disordered state [22]. In contrast, the excitation peak at 533 nm has a very large width: about 7 nm.

To find out why the short-wavelength part of the Eu^{3+} excitation spectrum was inefficient, we additionally measured the absorption spectrum (Fig. 6) of a

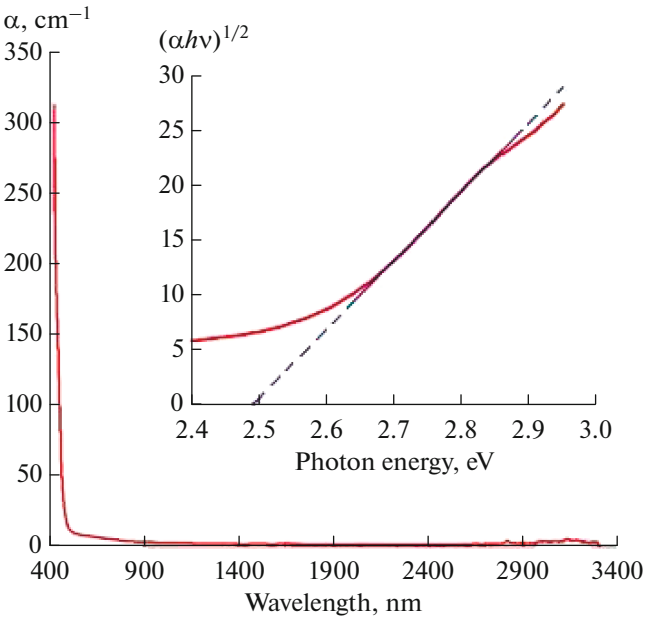

Fig. 6. Absorption spectrum of single-crystal $Pb_5(GeO_4)(VO_4)_2$. Inset: Tauc plot for an allowed indirect transition (α is the absorption coefficient).

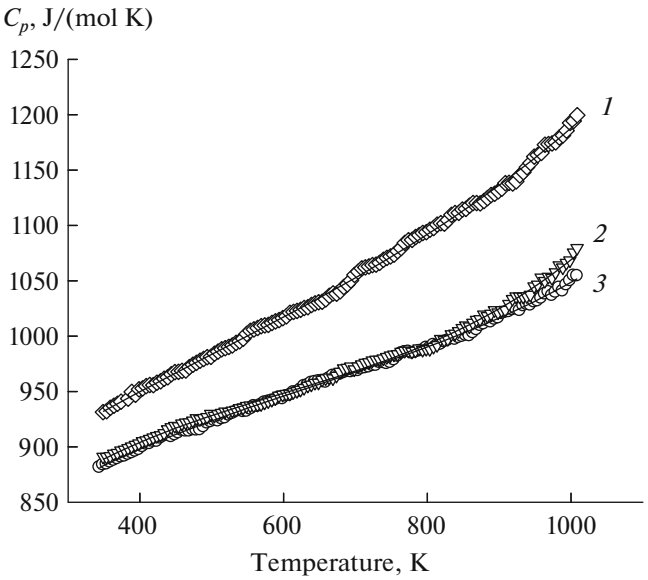

Fig. 7. Effect of temperature on the molar heat capacity of $Pb_{10-x}Eu_x(GeO_4)_{2+x}(VO_4)_{4-x}$ with $x = (1)$ 0.3, (2) 0.2, and (3) 0.3.

$Pb_5(GeO_4)(VO_4)_2$ single crystal (grown by the Czochralski technique as described by Gospodinov and Sveshtarov [23]).

The $Pb_5(GeO_4)(VO_4)_2$ crystal, containing no europium (host), was found to be transparent in the range from 3.3 μm to approximately 450 nm. Its band gap, as evaluated using a Tauc plot [24, 25] for an allowed indirect transition (Fig. 6, inset), is about 2.49 eV, and the main absorption around 400 nm is most likely due to VO groups. The drop in Eu^{3+} excitation efficiency around 400 nm and at shorter wavelengths can then be accounted for by energy transfer from Eu^{3+} to VO groups, followed by nonradiative relaxation in the conduction band and an indirect transition to the valence band.

Figure 7 illustrates the effect of temperature on the molar heat capacity of the Eu-substituted lead germanatovanadates. We call attention to the fact that the substituted apatites with $x = 0.1$ and 0.2 are very simi-

Table 4. Thermodynamic properties of $Pb_{9.7}Eu_{0.3}(GeO_4)_{2.3}(VO_4)_{3.7}$

T, K	C_p, J/(mol K)	$H°(T) - H°(350\ K)$, kJ/mol	$S°(T) - S°(350\ K)$, J/(mol K)	$-\Delta G/T*$, J/(mol K)
350	932.4	–	–	–
400	949.8	47.06	125.6	8.00
450	966.8	94.97	238.5	27.45
500	983.6	143.7	341.2	53.77
550	1000	193.3	435.8	84.25
600	1017	243.8	523.5	117.2
650	1035	295.1	605.6	151.7
700	1053	347.2	683.0	186.9
750	1072	400.3	756.2	222.4
800	1092	454.4	826.0	258.2
850	1113	509.6	892.9	293.4
900	1136	565.8	957.1	328.5
950	1161	623.2	1019	363.2
1000	1188	681.9	1079	397.5

* $\Delta G/T = [H°(T) - H°(350\ K)]/T - [S°(T) - S°(350)]$.

lar in heat capacity over the entire temperature range studied (350–1000 K).

The temperature-dependent molar heat capacity data for all of the $Pb_{10-x}Eu_x(GeO_4)_{2+x}(VO_4)_{4-x}$ apatites studied by us are well described by the Prausnitz–Reid–Sherwood equation [26]:

$$C_p = (717.6 \pm 7.7) + (682.7 \pm 37.2)\times10^{-3}T - (73.03 \pm 5.72)\times10^{-5}T^2 + (3.79 \pm 0.28)\times10^{-7}T^3 \quad (1)$$

for $x = 0.1$,

$$C_p = (684.9 \pm 10.4) + (925.7 \pm 5.02)\times10^{-3}T - (121.4 \pm 7.68)\times10^{-5}T^2 + (6.72 \pm 0.37)\times10^{-7}T^3 \quad (2)$$

for $x = 0.2$, and

$$C_p = (778.8267 \pm 12.9) + (559.1 \pm 5.99)\times10^{-3}T - (44.86 \pm 5.9)\times10^{-5}T^2 + (2.98 \pm 0.43)\times10^{-7}T^3 \quad (3)$$

for $x = 0.3$.

The correlation coefficients for Eqs. (1)–(3) are 0.9992, 0.9988, and 0.9993, respectively. Using these equations and well-known thermodynamic relations [26], we evaluated the enthalpy increment, entropy, and Gibbs energy of the apatites. As an example, Table 4 presents the C_p, $H°(T) - H°(350\ K)$, $S°(T) - S°(350\ K)$, and $-\Delta G/T*$ data for the sample with the composition $Pb_{9.7}Eu_{0.3}(GeO_4)_{2.3}(VO_4)_{3.7}$.

CONCLUSIONS

$Pb_{10-x}Eu_x(GeO_4)_{2+x}(VO_4)_{4-x}$ Eu-substituted lead germanatovanadates with different europium concentrations ($x = 0.1, 0.2, 0.3$) have been prepared by solid-state reactions using oxides as starting materials. The atomic position coordinates, isotropic thermal parameters, and principal bond lengths in the materials have been determined by X-ray diffraction, and we have refined the crystal structure of the synthesized apatite-like phases, (sp. gr. $P6_3/m$). The unit-cell parameters and density of the compounds have been determined as functions of europium concentration. We have studied the luminescence spectra of the $Pb_{10-x}Eu_x(GeO_4)_{2+x}(VO_4)_{4-x}$ ($x = 0.1, 0.2, 0.3$) materials and shown that the Eu^{3+} ions reside predominantly on the Pb1 site. According to the heat capacity data obtained for the samples by differential scanning calorimetry, the synthesized compounds are thermally stable throughout the temperature range studied (350–1000 K). C_p, $H°(T) - H°(350\ K)$, $S°(T) - S°(350\ K)$, and $-\Delta G/T*$ data are presented for a phase with the composition $Pb_{9.7}Eu_{0.3}(GeO_4)_{2.3}(VO_4)_{3.7}$.

ACKNOWLEDGMENTS

We are grateful to the Krasnoyarsk Regional Shared Research Facilities Center, Krasnoyarsk Scientific Center (Federal Research Center), Siberian Branch, Russian Academy of Sciences.

FUNDING

This work was supported in part by the Russian Federation Ministry of Science and Higher Education as part of the state research target for the Siberian Federal University federal state autonomous educational institution of higher education, project no. FSRZ-2020-0013.

REFERENCES

1. Yano, T., Nabeta, Y., and Watanabe, A., A new crystal $Pb_5(GeO_4)(VO_4)_2$ for acousto-optic applications, *Appl. Phys. Lett.,* 1971, vol. 18, no. 12, pp. 570–571.
2. Ivanov, A., Crystal structure refinement of $Pb_5(GeO_4)(VO_4)_2$ using X-ray powder diffraction peak profiles, *Zh. Strukt. Khim.,* 1990, vol. 31, no. 4, pp. 80–84.
3. Pasero, M., Kampf, A.R., Ferraris, C., et al., Nomenclature of the apatite supergroup minerals, *J. Mineral.,* 2010, vol. 22, pp. 163–179. https://doi.org/10.1127/0935-1221/2010/0022-2022
4. Baikie, T., Pramana, S.S., Ferraris, C., et al., Polysomatic apatites, *Acta Crystallogr., Sect. B: Struct. Sci.,* 2010, vol. 66, pp. 1–16. https://doi.org/10.1107/S0108768109053981
5. Yablochkova, N.V., Synthesis of $Pb_8Pr_2(GeO_4)_4(VO_4)_2$ and refinement of its crystal structure, *Russ. J. Inorg. Chem.,* 2013, vol. 58, no. 7, pp. 769–772. https://doi.org/10.1134/S0036023613070255
6. Ptáček, P., Opravil, T., Soukal, F., et al., Formation of strontium–yttrium germanium anionic lacunar apatite ($Sr_{2+\delta}Y_{6.67+(2\delta/3)}[GeO_4]_6O_{2\delta}$) as the intermediate phase of oxygen-rich yttrium–germanium apatite ($Y_{9.333+\varepsilon}[GeO_4]_{2+3/2\varepsilon}$), *Ceram. Int.,* 2017, vol. 43, pp. 7827–7838. https://doi.org/10.1016/j.ceramint.2017.03.097
7. Bulanov, E.N., Korshak, K.S., Lelet, M.I., et al., Bi-apatite: synthesis, crystal structure and low-temperature heat capacity, *J. Chem. Thermodyn.,* 2018, vol. 124, pp. 74–78. https://doi.org/10.1016/j/jct.2018.04.021
8. Kanazawa, T., *Inorganic Phosphate Materials,* Materials Science Monographs, vol. 52, Amsterdam: Elsevier, 1989.
9. Chakroun-Ouadhour, E., Ternane, R., Ben Hassen-Chekimi, D., et al., Synthesis, characterization and electrical properties of a lead sodium vanadate apatite, *Mater. Res. Bull.,* 2008, vol. 43, pp. 2451–2456. https://doi.org/10.1016/j.materresbull.2007.07.030
10. Zhuravlev, V.D and Velikodny, Yu.A., Lead lanthanum and strontium lanthanum germanovanadates with apatite and oxyapatite structures, *Russ. J. Inorg. Chem.,* 2009, vol. 54, no. 10, pp. 1551–1552.
11. Savankova, T.M., Akselrud, L.G., Ardanova, L.I., et al., Synthesis, crystal structure refinement, and elec-

trical conductivity of $Pb_{(8-x)}Na_2Sm_x(VO_4)_6O_{(x/2)}$, *J. Chem.,* 2014, pp. 1–7. https://doi.org/10.1155/2014/263548

12. Benmoussa, H., Mikou, M., Bensaoud, A., et al., Electrical properties of lanthanum containing vanadocalcic oxyapatite, *Mater. Res. Bull.,* 2000, vol. 35, pp. 369–375.
13. Nakayama, S., Higuchi, Y., Kondo, Y., et al., Effects of cation- or oxide ion-defect on conductivities of apatite-type La–Ge–O system ceramics, *Solid State Ionics,* 2004, vol. 170, pp. 219–223. https://doi.org/10.1016/j.ssi.2004.02.023
14. Denisova, L.T., Kargin, Yu.F., Golubeva, E.O., et al., Heat capacity of $Pb_{10-x}Pr_x(GeO_4)_{2+x}(VO_4)_{4-x}$ (x = 0, 1, 2, 3) apatites in the range 350–1050 K, *Inorg. Mater.,* 2020, vol. 56, no. 10. pp. 1027–1032. https://doi.org/10.1134/S0020168520100039
15. Denisova, L.T., Golubeva, E.O., Denisov, V.M., et al., High-temperature heat capacity of $Pb_9R(GeO_4)_3(VO_4)_3$ (R = La, Pr, Nd, Sm) apatites, *J. Phys. Chem. A,* 2020, vol. 94, no. 13, pp. 46–50. https://doi.org/10.1134/S0036024420130099
16. Ivanov, S.A. and Zavodnik, V.E., Crystal structure of $Pb_5GeV_2O_{12}$, *Kristallografiya,* 1989, vol. 34, no. 4, pp. 824–828.
17. Savankova, T.M., Ignatov, A.V., Utochkin, D.M., et al., Synthesis and characterization of $Pb_{(8-x)}Eu_x$-$Na_2(VO_4)_6O_{(x/2)}$ solid solutions, *Nauk. Pratsi DonNTU, Ser. Khim. Khim. Tekhnol.,* 2014, no. 2 (23), pp. 78–82.
18. *Bruker AXS TOPAS V4: General Profile and Structure Analysis Software for Powder Diffraction Data – User's Manual,* Karlsruhe: Bruker AXS, 2008.
19. Denisova, L.T., Irtyugo, L.A., Kargin, Yu.F., Beletskii, V.V., and Denisov, V.M., High-temperature heat capacity and thermodynamic properties of $Tb_2Sn_2O_7$, *Inorg. Mater.,* 2017, vol. 53, no. 1, pp. 93–95. https://doi.org/10.1134/S0020168517010046
20. Get'man, E.I., Yablochkova, N.V., Loboda, S.N., et al., Isomorphous substitution of europium for strontium in the structure of synthetic hydroxovanadate, *J. Solid State Chem.,* 2008, vol. 181, pp. 2386–2392. https://doi.org/10.1016/j.jssc.2008.06.003
21. Shannon, R.D., Revised effective ionic radii and systematic studies of interatomic distances in halides and chalcogenides, *Acta Crystallogr., Sect. A: Cryst. Phys., Diffr., Theor. Gen. Crystallogr.,* 1976, vol. 32, no. 5, pp. 751–767.
22. Krut'ko, V.A., Komova, M.G., and Popov, A.V., Synthesis of IR phosphors based on germanatoborate $Gd_{14}Ge_2B_6O_{34}$, *Russ. J. Inorg. Chem.,* 2016, vol. 61, no. 2, pp. 142–148. https://doi.org/10.1134/S003602361602011X
23. Gospodinov, M. and Sveshtarov, P., Growth of large $Pb_5GeO_4(VO_4)_2$, *Cryst. Res. Technol.,* 1990, vol. 25, no. 3, pp. K58–K61.
24. Tauc, J., Grigorovici, R., and Vancu, A., Optical properties and electronic structure of amorphous germanium, *Phys. Status Solidi,* 1966, vol. 15, pp. 627–637. https://doi.org/10.1002/pssb.19660150224
25. Domashevskaya, E.P., Ivkov, S.A., al-Haylani Hasan Ismail Dambos, and Ryabtsev, S.V., Effect of process conditions on the structure and optical properties of MoO_3 produced by vapor transport deposition, *Inorg. Mater.,* 2019, vol. 55, no. 1, pp. 49–58.
26. Chudnenko, K.V., *Termodinamicheskoe modelirovanie v geokhimii: teoriya, algoritmy, programmnoe obespechenie, prilozheniya* (Thermodynamic Modeling in Geochemistry: Theory, Algorithms, Software, and Applications), Novosibirsk: Geo, 2010.

Translated by O. Tsarev